AFRL-AFOSR-UK-TR-2013-0005

Effects of passive porous walls on the first mode of hypersonic boundary layers over a sharp cone

Professor Sharon O. Stephen

University of Birmingham
Edgbaston
Birmingham B15 2TT United Kingdom

EOARD Grant 12-2110

Report Date: January 2013

Final Report from 01 August 2012 to 31 January 2013

Air Force Research Laboratory
Air Force Office of Scientific Research
European Office of Aerospace Research and Development
Unit 4515 Box 14, APO AE 09421

REPORT DOCUMENTATION PAGE

Form Approved OMB No. 0704-0188

1. REPORT DATE *(DD-MM-YYYY)*	2. REPORT TYPE	3. DATES COVERED *(From – To)*
30-01-2013	Final Report	1 August 2012 – 31 January 2013

4. TITLE AND SUBTITLE

Effects of passive porous walls on the first mode of hypersonic boundary layers over a sharp cone

5a. CONTRACT NUMBER

FA8655-12-1-2110

5b. GRANT NUMBER

Grant 12-2110

5c. PROGRAM ELEMENT NUMBER

61102F

6. AUTHOR(S)

Professor Sharon O. Stephen

5d. PROJECT NUMBER

5d. TASK NUMBER

5e. WORK UNIT NUMBER

7. PERFORMING ORGANIZATION NAME(S) AND ADDRESS(ES)

University of Birmingham
Edgbaston
Birmingham B15 2TT United Kingdom

8. PERFORMING ORGANIZATION REPORT NUMBER

N/A

9. SPONSORING/MONITORING AGENCY NAME(S) AND ADDRESS(ES)

EOARD
Unit 4515 BOX 14
APO AE 09421

10. SPONSOR/MONITOR'S ACRONYM(S)

AFRL/AFOSR/IOE (EOARD)

11. SPONSOR/MONITOR'S REPORT NUMBER(S)

AFRL-AFOSR-UK-TR-2013-0005

12. DISTRIBUTION/AVAILABILITY STATEMENT

Distribution A: Approved for public release; distribution is unlimited.

13. SUPPLEMENTARY NOTES

14. ABSTRACT

A theoretical linear stability analysis is used to consider the effect of a porous wall on the first Mack mode of a hypersonic boundary layer on a sharp slender cone. The effect of curvature and of the attached shock are included for axisymmetric and non-axisymmetric disturbances. The flow in the hypersonic boundary layer is coupled to the flow in the porous layer by the porous wall model admittance. We considered the effect of the phase angle of the admittance of a circular pore model on the first Mack mode. We further considered the effect of two other wall models, a high porosity rectangular mesh microstructure model and a low porosity model comprising of spanwise grooves with varying thickness, on the linear and weakly nonlinear stability of the flow.

15. SUBJECT TERMS

EOARD, porous walls, boundary layer, hypersonics, sharp cone

16. SECURITY CLASSIFICATION OF:			17. LIMITATION OF ABSTRACT	18, NUMBER OF PAGES	19a. NAME OF RESPONSIBLE PERSON
a. REPORT	b. ABSTRACT	c. THIS PAGE			Gregg Abate
UNCLAS	UNCLAS	UNCLAS	SAR	32	19b. TELEPHONE NUMBER *(Include area code)* +44 (0)1895 616021

Effects of passive porous walls on the first mode of hypersonic boundary layers over a sharp cone

Principal investigator: Sharon O. Stephen,
Research Assistant: Vipin Michael,
School of Mathematics, University of Birmingham, U.K.

Report for Grant award no. FA8655-12-1-2110
Government Program Manager: Dr. Gregg Abate
Award period: 1 August 2012 to 31 January 2013

Contents

List of Figures

Summary

A theoretical linear stability analysis is used to consider the effect of a porous wall on the first Mack mode of a hypersonic boundary layer on a sharp slender cone. The effect of curvature and of the attached shock are included for axisymmetric and non-axisymmetric disturbances. The flow in the hypersonic boundary layer is coupled to the flow in the porous layer by the porous wall model admittance. We considered the effect of the phase angle of the admittance of a circular pore model on the first Mack mode. We further considered the effect of two other wall models, a high porosity rectangular mesh microstructure model and a low porosity model comprising of spanwise grooves with varying thickness, on the linear and weakly nonlinear stability of the flow.

1 Introduction

Transition to turbulence in hypersonic flows is associated with amplification of the first and/or second Mack modes. The first Mack mode is the high speed counterpart of Tollmien–Schlichting waves, so a viscous instability, with modes located close to the boundary. The second Mack mode is an inviscid instability. The second Mack mode is believed to be responsible for transition to turbulence on hypersonic slender bodies. Recent experiments by Fedorov *et al.* [1, 2, 3] have shown that a porous coating greatly stabilizes the second mode of the hypersonic boundary layer on sharp slender cones. The effect of the porous coating is to reduce the growth rates of the second mode to a level where they are comparable with those of the first mode (occurring at lower frequencies). In addition, the first mode is observed to be slightly destabilized by the presence of the porous coating. Thus, the first mode may now be more significant in the transition process.

We consider the effect of porous walls on the linear instability and weakly nonlinear stability of hypersonic flow over a sharp slender cone. In this theoretical and asymptotic investigation for large Mach number and large Reynolds number the scales used will be appropriate to the first mode instability which is governed by a triple-deck structure. The effects of curvature and the attached shock will be taken into account. The effect of the porous wall will change the boundary condition on the normal velocity at the interface.

Our previous studies considered the effect of various porous wall models reported in literature. The eigenrelations governing the linear stability of the problem was derived. Neutral and spatial instability results show the presence of multiple unstable modes and the destabilising effect of the porous wall models on them. The weakly nonlinear stability analysis carried out allows an equation for the amplitude of disturbances to be derived. The stabilising or destabilising effect of nonlinearity is found to depend on the cone radius. It was shown that porous walls significantly influences the effect of nonlinearity.

The effect of the attached shock was shown to be significant [4]. In the absence of a shock, unstable solutions are possible only for a finite range of cone radii and nonlinearity stabilises linearly unstable disturbances for all admissible values of the cone radius. The presence of the shock leads to multiple unstable modes for all values of the cone radius. The influence of curvature is also important. Curvature was shown to enhance nonlinear effects [4].

Our previous results [5, 4] show that for sufficiently large cone radius, nonlinear effects destabilise all linearly unstable viscous modes on a solid cone surface. At small values of the radius, corresponding to typical lengths of models tested in wind tunnels, it is the unstable mode with the lowest frequency that is destabilised by nonlinearity. Spatial instability results demonstrate that these are the fastest growing disturbances but maximum growth rates are significantly smaller than the second Mack mode. This may explain why in experiments, transition has been observed due to the second Mack mode on solid cones. In the presence of porous walls, lower-frequency first Mack modes are also destabilised by nonlinearity while higher-frequency first Mack modes that are destabilised on the solid wall at a particular location now become stabilised for a range of local cone radii. This effect is enhanced by

models with higher porosity. Thus over porous surfaces we can expect interaction of first Mack modes in the low-frequency spectrum to lead to nonlinear amplification of disturbance amplitudes beyond the critical value.

Recently, parametric studies of porous wall models were reported with the focus on minimising the destabilising effect on the first Mack mode [6]. These authors have analysed the porous wall admittance and studied the effect of the admittance phase angle on Mack's first mode destabilisation. They investigated the variation of the phase angle of admittance with pore radius and thickness and show that there is a minimum phase angle indicating an optimal thickness or pore radius. Numerical simulations using the optimal pore radius indicate weaker destabilisation of the first mode [6].

In this report we consider the effect of the phase angle of the porous wall admittance on the linear and nonlinear stability of the flow. We compare our existing results with those obtained using a theoretical porous coating with purely real admittance. We then determine the optimum phase angle for minimum first mode destabilisation using actual regular microstructure porous coatings. We then investigate the effect of porosity on the nonlinear stability of the flow. Nonlinear stability results using the high porosity mesh microstructure model are presented. A novel low porosity coating proposed in the literature [7] is then considered.

2 Methods, Assumptions, and Procedures

2.1 Basic flow

The flow of a compressible, viscous fluid over a sharp cone with a porous boundary, of semi-angle θ_c is considered at hypersonic speeds, with magnitude U_0 parallel to its axis. We consider an attached conical shock which makes an angle θ_s with the cone; a situation which is illustrated in figure 1. Spherical polars (x, θ, ϕ) is the natural coordinate system in which to describe the basic flow, and here ϕ denotes the azimuthal angle. Furthermore, the radial distance x has been non-dimensionalised with respect to L^*, the distance from the tip of the cone to the location under consideration.

The approximate basic flow used is described in [8] so the complete details are omitted. The important features are summarised below. Away from the surface of the cone the flow satisfies the (inviscid) Euler equations. The velocities are non-dimensionalised with respect to U_-, where U_- is the magnitude of the fluid velocity just behind the shock. Additionally, the time, pressure and density are non-dimensionalised with respect to L^*/U_-, $\rho_- U_-^2$ and ρ_- respectively, where ρ_- is the density just behind the shock. Finally, the basic temperature is non-dimensionalised by T_-, the temperature just behind the shock.

The inviscid axisymmetric flow between the cone surface and the conical shock depends only on the polar angle θ. The jump conditions at the shock must be considered and the velocity components may be obtained from a numerical solution of the Taylor-Maccoll equation [9]. Since, for a hypersonic flow over a slender cone, the density does not vary much, we use the steady, constant-density solution given by [10], which has the advantage of analytical

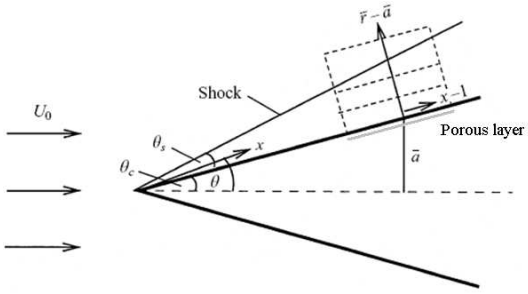

Figure 1: The geometry of the cone and shock. The cone is taken to be of semi-angle θ_c with the attached conical shock making an angle θ_s with the surface of the cone.

expressions for the velocity components and pressure. For a slender cone and hypersonic speeds these approximate solutions agree well with the exact (numerical) solutions.

This solution is not valid close to the surface of the cone so a boundary-layer solution has to be introduced in this region. The Reynolds number of the flow is defined by $Re = \rho_- U_- L^*/\mu_-$. Taking the angle of the cone to be small the governing equations in the boundary-layer region are given in [8] in terms of dimensionless coordinates $(x, \overline{r}, \phi)$ and the Mach number, M, just behind the shock. Then $L^*\overline{r}$ is the normal direction to the cone surface, where $\overline{r} = \overline{a}$ on the generator of the cone. The corresponding non-dimensional velocities are (u, v, w) and the non-dimensionalised pressure and density p and ρ, respectively. The boundary conditions are no-slip at the surface of the cone (coupled to the porous layer) and appropriate conditions at the shock location. The non-dimensional temperature and viscosity at the surface of the cone are taken to be T_w and μ_w, respectively.

2.2 Porous boundary

We will present results corresponding to porous surfaces used in the previous experimental investigations [2, 11, 12]. In all cases the porous layer admittance A_y can then be expressed in the form

$$A_y = -(\phi_0/Z_0)\tanh(\Lambda h_0), \tag{1}$$

where ϕ_0 is the porosity and h_0 is the non-dimensional thickness of the porous layer. The porous layer parameters are non-dimensionalised with respect to the boundary-layer displacement thickness δ^* which is approximated using the Blasius length scale $\delta^* = \sqrt{L^*/Re_1}$, where Re_1 is the unit Reynolds number at the outer edge of the boundary layer (just below the shock). Z_0 and Λ are the characteristic impedance and propagation constant of an isolated pore, respectively. Fedorov *et al.* [3] give the following expressions for the porous layer characteristics:

$$Z_0 = \frac{\sqrt{\rho_D/C_D}}{M\sqrt{T_w}} \quad \text{and} \quad \Lambda = \frac{\mathrm{i}\omega M}{\sqrt{T_w}}\sqrt{\rho_D C_D}, \tag{2}$$

where ω is the disturbance frequency. These are functions of the complex dynamic density ρ_D and complex dynamic compressibility C_D. The precise definitions of these quantities

depends on the structure of the porous wall. Following [1, 3] we consider the porous layer on the cone surface to be a sheet of thickness h^* perforated with cylindrical blind holes of radius r_p^* and equal spacing $s^* = r_p^*\sqrt{\pi/\phi_0}$. This model takes into account gas rarefaction effects. We have

$$\left.\begin{aligned} &\rho_D = \frac{1}{1-F(B_\nu,\zeta)}, \quad C_D = 1+(\gamma-1)F(B_E,\zeta\sqrt{Pr}), \\ &F(B_\nu,\zeta) = \frac{G(\zeta)}{1-0.5B_\nu\zeta^2G(\zeta)}, \quad F(B_E,\zeta\sqrt{Pr}) = \frac{G(\zeta\sqrt{Pr})}{1-0.5B_E(\zeta\sqrt{Pr})^2G(\zeta\sqrt{Pr})}, \end{aligned}\right\} \tag{3}$$

where

$$B_\nu = (2\alpha_\nu^{-1}-1)Kn, \quad B_E = [\gamma(2\alpha_E^{-1}-1)/(\gamma+1)Pr]Kn, \quad G(\zeta) = \frac{2J_1(\zeta)}{\zeta J_0(\zeta)}, \tag{4}$$

where $\zeta = r_p\sqrt{\mathrm{i}\omega\rho_w R/\mu_w}$ and γ is the specific heat ratio of air. Here $J_{0,1}$ are Bessel functions of the first kind, α_ν and α_E are molecular accommodation coefficients, Kn is the Knudsen number, Pr is the Prandtl number and R is the Reynolds number based on boundary-layer displacement thickness of the gas flow.

Following [12] we can also consider the porous coating on the cone surface to comprise of several layers of stainless steel wire mesh as shown in Figure 3 of their paper. A similar model to the one described above for a regular microstructure is employed. Following [13] we have different expressions for the complex dynamic density and compressibility. We then obtain the following expressions for the porous layer characteristics for a square mesh microstructure:

$$\left.\begin{aligned} &\rho_D = 1/(1-F(\zeta)), \qquad C_D = 1+(\gamma-1)F(\widetilde{\zeta}), \\ &F(\zeta) = 1+\zeta^2\sum_{m=0}^{\infty}\left[\frac{2}{\gamma_m^2\beta_m^2}\Big(1-\frac{\tanh(\beta_m)}{\beta_m}\Big)\right], \\ &F(\widetilde{\zeta}) = 1+\widetilde{\zeta}^2\sum_{m=0}^{\infty}\left[\frac{2}{\gamma_m^2\widetilde{\beta_m}^2}\Big(1-\frac{\tanh(\widetilde{\beta_m})}{\widetilde{\beta_m}}\Big)\right], \end{aligned}\right\} \tag{5}$$

where

$$\gamma_m = \pi(m+\frac{1}{2}), \qquad \beta_m = \sqrt{(\gamma_m^2-\zeta^2)}, \qquad \widetilde{\beta_m} = \sqrt{(\gamma_m^2-\widetilde{\zeta}^2)}. \tag{6}$$

The characteristic size of an isolated pore is given by

$$\zeta = \sqrt{\frac{i\omega\rho_w\widetilde{a}^2}{\mu_w}R}, \quad \text{and} \quad \widetilde{\zeta} = \sqrt{Pr}\zeta. \tag{7}$$

In the subsequent stability calculations we take

$$M_- = 5.3, \quad T_-^* = 56.4K, \quad Pr = 0.708,$$

$$Re_1 = 15.2\times10^6, \quad Re = Re_1L^*, \quad R = \sqrt{Re},$$

$$T_w = T_{ad}, \quad T_{ad} = 1 + \sqrt{Pr}\frac{\gamma - 1}{2}M_-^2,$$
$$\rho_w = \frac{1}{T_w}, \quad \mu_w(T_w) = \frac{1+S}{T_w + S}T_w^{3/2}, \quad S = \frac{110}{T_-^*}.$$

Following [1] we consider $h_0 \gg r_p$. The last relation implies that $\Lambda h_0 \to \infty$, and so our admittance equation (1) may be simplified to

$$A_y = -\phi_0/Z_0. \tag{8}$$

The wall boundary condition is given by

$$v = A_y\left(p - p_-\right), \tag{9}$$

where $p_- = \gamma^{-1}M^{-2}$.

3 Linear stability problem

The linear stability of the basic flow described in § 2.1 for $M \gg 1$ and $Re \gg 1$ is investigated in the weak-interaction region following a triple-deck formulation used by [14] and [15]. The conditions to be satisfied at the shock by a disturbance to this basic flow must be specified and these have been derived in detail in [16]. The requisite constraints were obtained by considering the linearised jump conditions at the shock for infinitesimal waves beneath the shock; a similar procedure was adopted by [14] for flow over a wedge. Although the basic flow is not uniform in the regions below and above the shock, [16] showed that the jump conditions may still be evaluated at the undisturbed position of the shock. The condition satisfied by the pressure amplitudes of the two acoustic waves (which are incident and reflected from the shock) is found to be similar to that for a wedge obtained by [14].

Attention is focused at a location on the surface of the cone with non-dimensional radius $\overline{a} = a^*/L^*$. It is assumed that $\overline{a}Re^{\frac{3}{8}}M^{\frac{1}{4}}\mu_w^{-\frac{3}{8}}T_w^{-\frac{9}{8}} = a \sim O(1)$ denotes the scale of the radius at this point; thus we have chosen $\sin\theta_c \sim \theta_c \sim Re^{-\frac{3}{8}}M^{-\frac{1}{4}}\mu_w^{\frac{3}{8}}T_w^{\frac{9}{8}}$.

Our study is confined to the question of the stability of the flow at a location on the body where the boundary-layer thickness is $O(Re^{-\frac{1}{2}}L^*)$, which is thin compared to the local radius of the cone. This situation is chosen so that curvature effects are significant. The analysis is somewhat simplified if non-parallel effects can be neglected and [14] showed that this is justifiable if the 'Newtonian' assumption $\gamma - 1 \ll 1$ is made. Thus, for simplicity, this condition is taken to hold in the following analysis although it can be easily relaxed for more involved studies.

It is convenient to scale out some of the parameters in the problem, namely μ_w, T_w and λ, where the last quantity denotes the boundary-layer skin friction. For axisymmetric flow the Mach number may be scaled out of the linear stability problem.

We consider perturbations proportional to

$$E = \exp\left[\mathrm{i}\left(\alpha X + n\phi - \Omega\tau\right)\right],$$

where α and n are the streamwise and azimuthal wavenumbers respectively and Ω is the frequency of the disturbance. Note that n is an integer.

Previous scaling, following [14] and [17], is applied to the resulting equations for axisymmetric disturbances (corresponding to $n = 0$). Analytic solutions of these equations yields an eigenrelation relating the streamwise wavenumber α and frequency Ω, namely

$$\frac{\mathrm{Ai}'(\xi_0)}{\int_{\xi_0}^{\infty}\mathrm{Ai}(\xi)\mathrm{d}\xi} = -(\mathrm{i}\alpha)^{1/3}\left(\overline{A_Y} + \mathrm{i}\alpha\right)\frac{I_0(\mathrm{i}\alpha r_s)K_0(\mathrm{i}\alpha a) - I_0(\mathrm{i}\alpha a)K_0(\mathrm{i}\alpha r_s)}{I_0(\mathrm{i}\alpha r_s)K_1(\mathrm{i}\alpha a) + I_1(\mathrm{i}\alpha a)K_0(\mathrm{i}\alpha r_s)}. \tag{10}$$

Here $\xi_0 = -\mathrm{i}^{1/3}\Omega\alpha^{-2/3}$, $\mathrm{Ai}(\xi)$ is the Airy function, $K_n(z)$ and $I_n(z)$ are the usual modified Bessel functions, and $A_y = Re^{-1/8}\mu_w^{1/8}\lambda^{1/4}T_w^{3/8}(M^2-1)^{3/8}\overline{A_Y}$. The admittance, A_y, is a function of the disturbance frequency and depends on the physical properties of the flow and the porous layer. The angular frequency of disturbance propagation through the pore is $\omega = (R/Re)Re^{1/4}\mu_w^{-1/4}\lambda^{3/2}T_w^{-3/4}(M^2-1)^{1/4}\Omega$. The parameter r_s is the scaled non-dimensional location of the shock. The values of a and r_s depend on the physical parameters for the flow. The relationship between r_s and a is discussed in [4] and [5]. The cone angle and Mach number will determine the shock angle θ_s and the scaled radius a. Then the scaled shock location r_s is determined using

$$\frac{a}{r_s} \approx \frac{\sin\theta_c}{\tan\theta_s + \sin\theta_c}. \tag{11}$$

For a free stream Mach number $M_\infty = 6$ flowing over a cone of half-angle $\theta_c = 6^0$, the above formula gives $a/r_s = 0.57$. All our stability results are presented using this ratio.

The stability analysis for non-axisymmetric disturbances with azimuthal wavenumber n is carried out in a similar manner to that just described for axisymmetric disturbances. The scaling is different and in particular

$$A_y = Re^{-1/8}\mu_w^{1/8}\lambda^{1/4}T_w^{3/8}M^{5/4}\overline{A_Y}$$

and

$$\omega = (R/Re)Re^{1/4}\mu_w^{-1/4}\lambda^{3/2}T_w^{-3/4}M^{-1/2}\Omega.$$

The resulting eigenrelation for non-axisymmetric disturbances is given by

$$\frac{\mathrm{Ai}'(\xi_0)}{\int_{\xi_0}^{\infty}\mathrm{Ai}(\xi)\mathrm{d}\xi} = (\mathrm{i}\alpha)^{1/3}\left[\overline{A_Y} + \frac{\mathrm{i}n^2}{\alpha a^2}\right]\frac{I_n(\mathrm{i}\alpha r_s)K_n(\mathrm{i}\alpha a) - I_n(\mathrm{i}\alpha a)K_n(\mathrm{i}\alpha r_s)}{I_n(\mathrm{i}\alpha r_s)K_n'(\mathrm{i}\alpha a) - I_n'(\mathrm{i}\alpha a)K_n(\mathrm{i}\alpha r_s)}. \tag{12}$$

4 Nonlinear stability problem

The linear stability analysis will not be valid for larger disturbances. Thus, it is important to determine the effect of nonlinearity on the stability of hypersonic boundary layer flow over a sharp slender cone with a porous wall. We consider a weakly nonlinear disturbance which develops in the vicinity of a linear neutral point (real α and Ω for fixed $n > 0$). If the relative amplitude of the disturbance in the lower deck of the triple-deck structure is $O(h)$,

$h \ll 1$, then the scaled amplitude A of the mode will evolve on an $O(h^2)$ lengthscale. Thus, we consider perturbations at the point

$$x = 1 + h^2 x_2.$$

Since the skin friction λ is a function of x we define it as $\lambda(x) = \lambda_1 + \ldots$ and slightly perturb it as follows.

$$\lambda = \lambda_1 + h^2 \lambda_2,$$

where $\lambda_2 = x_2 d\lambda/dx|_{x=1}$. Additionally, we choose to fix the azimuthal wavenumber and write

$$\Omega = \Omega_1 + h^2 \Omega_2,$$

where Ω_1 is the neutral value of Ω. To account for the slow modulation of the amplitude on streamwise lengthscales we introduce the coordinate

$$\tilde{X} = h^2 X,$$

and then by use of multiple scales we replace all X derivatives throughout according to

$$\frac{\partial}{\partial X} \to \frac{\partial}{\partial X} + h^2 \frac{\partial}{\partial \tilde{X}}.$$

Now for $h \ll 1$ we proceed to seek solutions of the lower-deck equations ((8) and (9) in the second report) and the upper-deck problem ((11) in the second report) where

$$\left(U - \left(1 + h^2 \lambda_2\right) Y, V, W, P, A, \tilde{p}\right) = \sum_{j=1}^{3} h^j \left(U_j, V_j, W_j, P_j, A_j, \tilde{p}_j\right) + O(h^4). \tag{13}$$

Substitution of (13) into the disturbance equations leads to a hierarchy of problems at increasing orders in h.

The solution for the $O(h)$ terms in (13) has been obtained from the linear stability analysis reported previously, resulting in the dispersion relations (10) and (12). The solution for A_1 has the form

$$A_1 = A_{11} E + A_{11}^{(c)} E^{-1},$$

where the superscript (c) denotes complex conjugate. At $O(h^2)$ we find the solution for A_2 takes the form

$$A_2 = A_{22} E^2 + A_{20} + A_{22}^{(c)} E^{-2},$$

with similar expansions for U_2, V_2, W_2, P_2 and $\tilde{p}_2$. The analysis follows that for the solid wall problem (see [18]) but the boundary condition at the porous wall leads to additional terms in the solutions. Solving the equations and satisfying all the boundary conditions leads to an expression relating the amplitude at $O(h^2)$ to the square of the amplitude at $O(h)$.

At $O(h^3)$ the amplitude equation for the unknown function $A_{11}(\tilde{X})$ is determined. This equation arises from a solvability condition on the $O(h^3 E)$ terms. We seek solutions of the form

$$\tilde{p}_3 = \tilde{p}_{31} E + \tilde{p}_{32} E^2 + \tilde{p}_{33} E^3 + \tilde{p}_{31}^{(c)} E^{-1} + \tilde{p}_{32}^{(c)} E^{-2} + \tilde{p}_{33}^{(c)} E^{-3} + \tilde{p}_{30}.$$

The solution in the lower deck involves an inhomogeneous differential equation of which a solution only exists if a certain compatibility condition holds. This condition is derived by considering the adjoint system of the problem as in [19]. Specifically, we multiply the inhomogeneous equation by the adjoint function and integrate over the range $[\xi_0, \infty]$.

By matching the solution for $\tilde{p}_{31}$ with the solution for the disturbance pressure in the main deck we obtain the evolution equation for A_{11} in the form

$$a_1 \frac{\mathrm{d}A_{11}}{\mathrm{d}\tilde{X}} = (a_2\lambda_2 + a_3\Omega_2)\, A_{11} + a_4 A_{11}|A_{11}|^2 \,. \tag{14}$$

The complex constants in (14) are defined in [4]. The coefficients are functions of the neutral results and so depend on the porous wall properties. The porous wall has introduced additional terms in the coefficients. Thus, their evaluation requires substantial numerical calculations.

The corresponding nonlinear stability problem for axisymmetric disturbances must be considered separately since the Mach number can be scaled out of the weakly nonlinear problem. The analysis is very similar to that for the non-axisymmetric problem and the resulting amplitude equation is presented in [4].

5 Results

5.1 Phase angle of admittance

We want to investigate the effect of the phase angle of the porous wall admittance A_y on the linear and nonlinear stability problem. We perform our stability calculations using an "artificial" porous coating with zero imaginary part of the admittance (phase angle = π). We call this quantity A_y^r.

Figure 2 shows the neutral solutions for Ω for $a/r_s = 0.57$ and $n = 1$ using a regular microstructure model with admittance A_y and admittance A_y^r. The flow is unstable above the neutral curves. We see that having a porous coating with phase angle π leads to lower neutral curves for the higher modes. So there is a destabilising effect in the sense that low frequencies may become unstable. Corresponding results for $n = 2$ is shown in figure 3. We see that the effect of the phase angle is small for these disturbances. We can look at the effect on axisymmetric disturbances in figure 4. We see that there is very little effect of the phase angle on the neutral modes.

We can now examine the effect of the phase angle on the spatial growth rates. We begin with figure 5 which shows the variation of the spatial growth rates with Ω for $n = 1$ for different values of a. We see that a phase angle of π leads to slight reduction of the maximum growth rates for all values of a. Corresponding results for $n = 2$ are shown in figure 6 where we observe similar trends. Finally we look at the effect of phase angle on the axisymmetric problem in figure 7. Here we see that a phase angle of π leads to a slight increase in maximum growth rates at larger values of a.

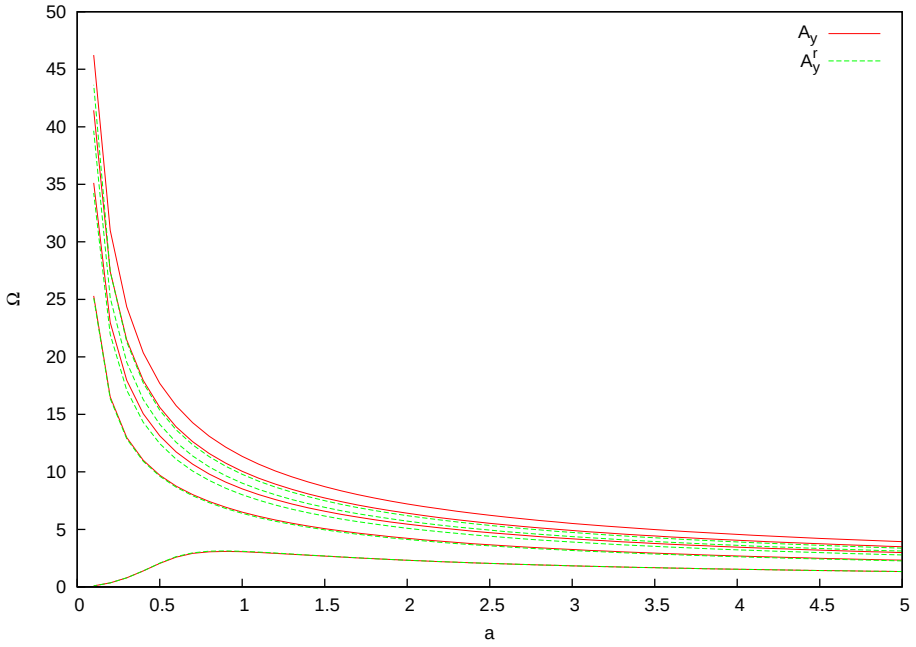

Figure 2: Variation of neutral values of frequency Ω for $n = 1$ and $a/r_s = 0.57$ with cone radius a for a regular microstructure model with admittance A_y and admittance A_y^r.

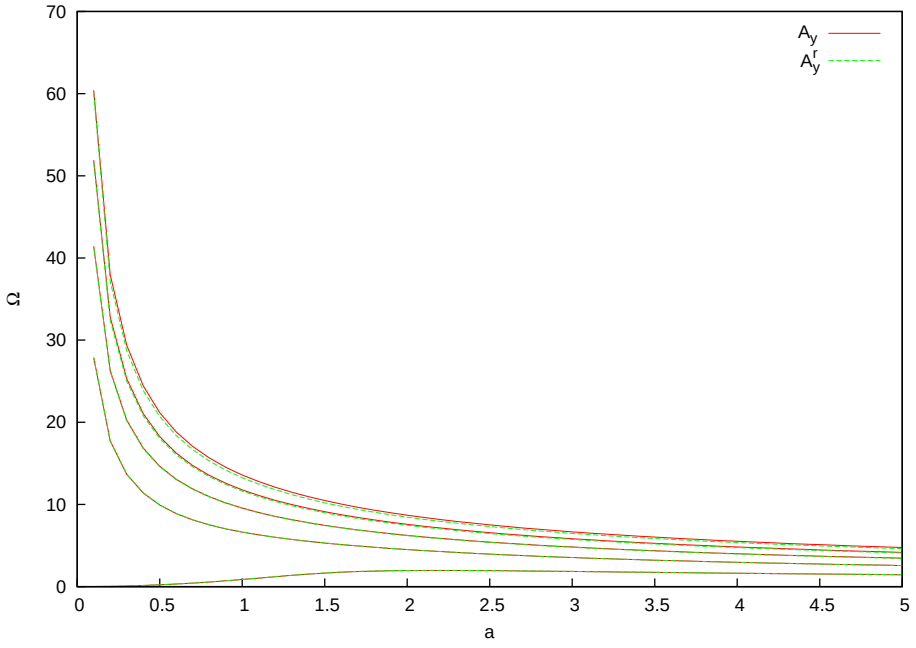

Figure 3: Variation of neutral values of frequency Ω for $n = 2$ and $a/r_s = 0.57$ with cone radius a for a regular microstructure model with admittance A_y and admittance A_y^r.

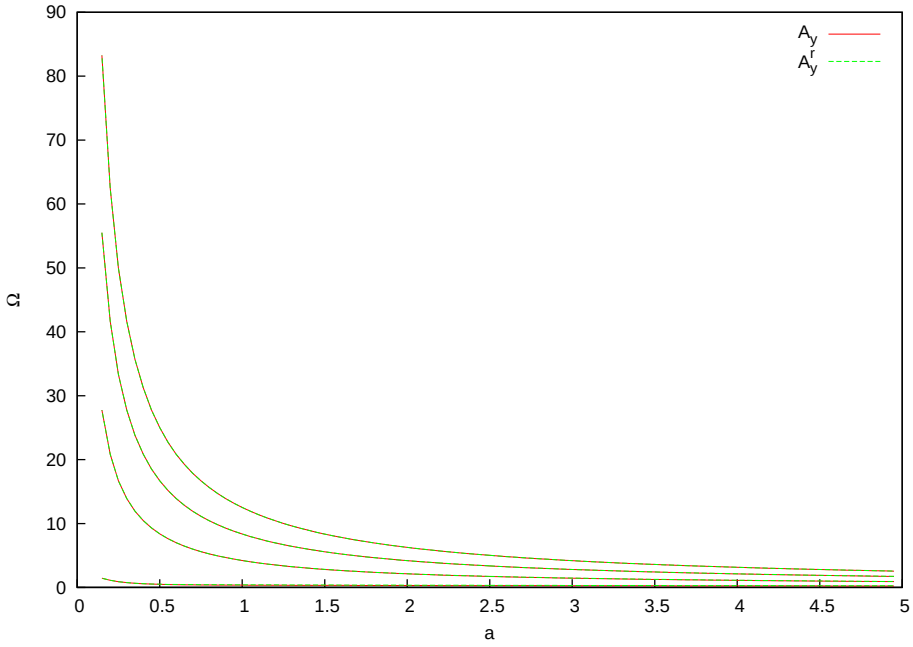

Figure 4: Variation of neutral values of frequency Ω for $n = 0$ and $a/r_s = 0.57$ with cone radius a for a regular microstructure model with admittance A_y and admittance A_y^r.

We now examine the effect of the phase angle on the nonlinear stability problem. We begin with figure 8 which shows $Re(a_4/a_1)$ for $n = 1$ and $a/r_s = 0.57$. We note that if $Re(a_4/a_1) > 0$, the nonlinear effects are destabilising. We see that a phase angle of π leads to a greater destabilising effect of nonlinearity. This can be seen by noting that $Re(a_4/a_1) > 0$ for smaller values of a for each mode. Corresponding results for $n = 2$ are shown in figure 9 where we notice a similar trend. Finally we look at the effect of phase angle on the axisymmetric problem in figure 10 and notice a similar effect to the non-axisymmetric case. We see that the effect of phase angle is more significant particularly for the first mode.

In the above calculations we considered a regular infinitely thick "artifical" coating with an admittance with zero imaginary part. We found that the effect of phase angle has a more significant effect on the nonlinear stability of both axisymmetric and non-axisymmetric disturbances. For "actual" porous coatings we examine the variation of the phase angle with pore radius r_p^*. Here we fix the porosity and assume that the thickness $h^* \gg r_p^*$. Let us consider the porous wall model equations (2-8) with $Kn = 0$. For small values of pore radius r_p we will assume that $|\zeta| \ll 1$. Then by using the appropriate small argument asymptotic expansions of the Bessel functions $J_0 \sim 1/2\zeta$ and $J_1 \sim 1-\zeta^2/4$ we can show that $G(\zeta) \sim 1+\zeta^2/4$. Thus we can approximate $\rho_D \sim -4/\zeta^2+\ldots$ and $C_D \sim \gamma+\ldots$. We can then show that $A_y \sim i\zeta = |A_y|e^{i3\pi/4}$. Let us now consider equations (2-8) for large values of pore radius r_p such that we can assume $|\zeta| \gg 1$. Now the large argument asymptotic expansions of the Bessel functions are $J_0 \sim \left(1/\sqrt{\pi\zeta}\right)(\cos\zeta + \sin\zeta)$ and $J_1 \sim \left(-1/\sqrt{\pi\zeta}\right)(\cos\zeta + \sin\zeta)$ leading to $G(\zeta) \sim -2/\zeta$. Using these results we can approximate $\rho_D \sim 1 - 2/\zeta + \ldots$ and $C_D \sim 1 - 2(\gamma - 1)/\zeta + \ldots$. We can then show that $A_y \sim \zeta^2 = |A_y|e^{i\pi}$.

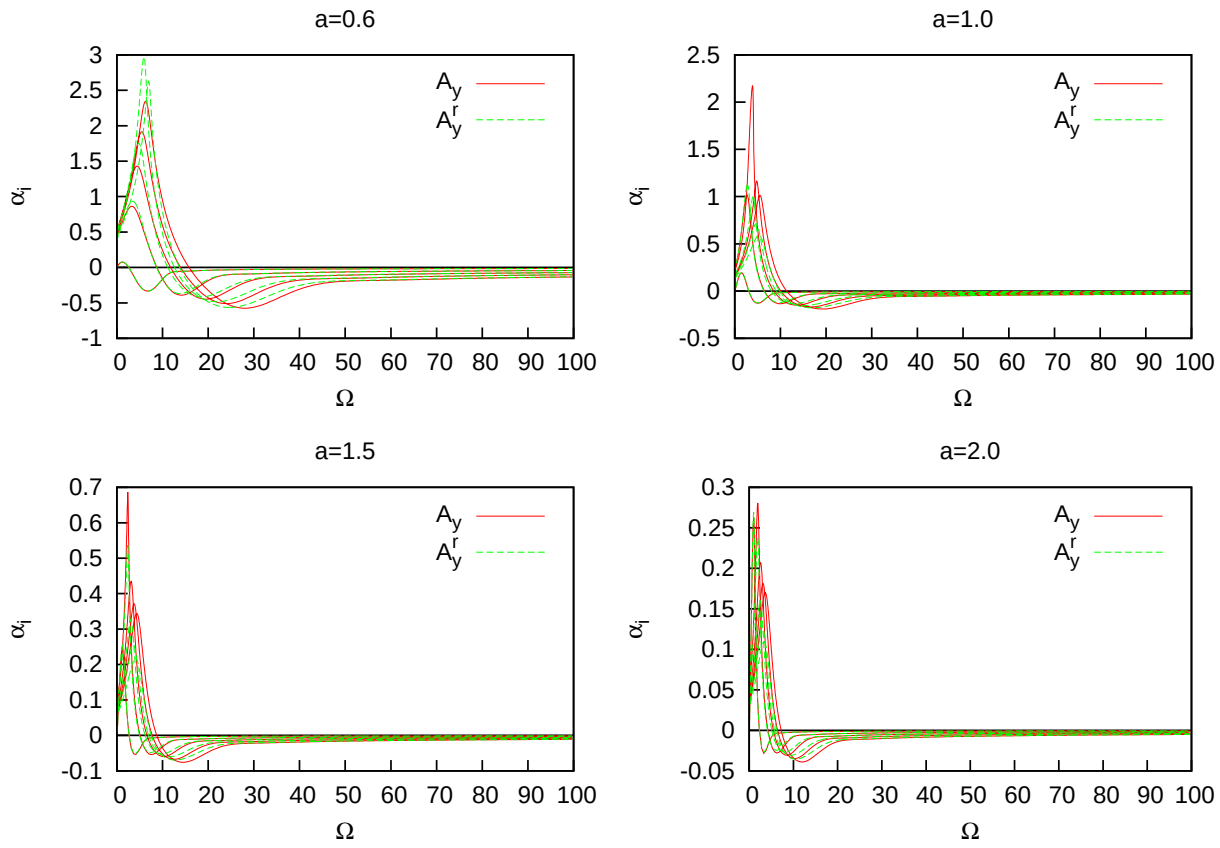

Figure 5: Variation of α_i for $n = 1$ and $a/r_s = 0.57$ with frequency Ω for a regular microstructure model with admittance A_y and admittance A_y^r.

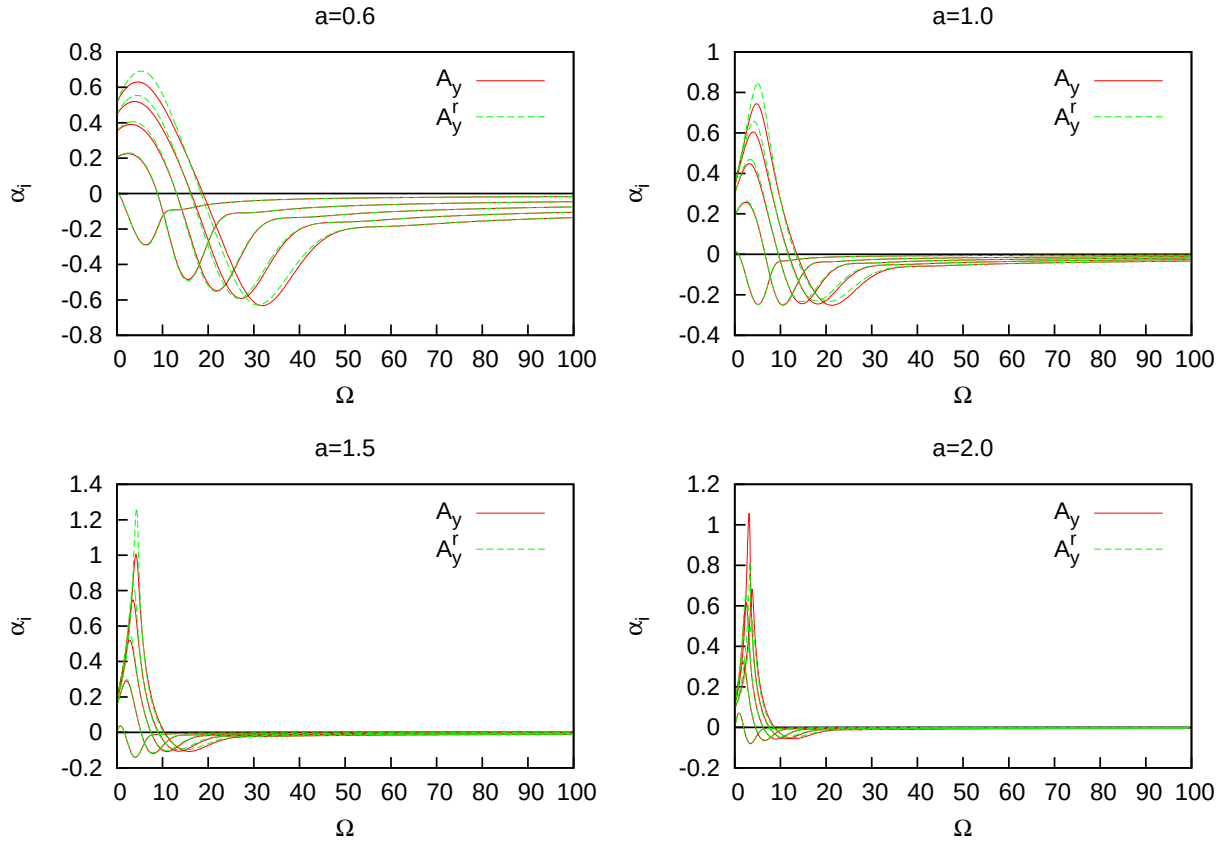

Figure 6: Variation of α_i for $n = 2$ and $a/r_s = 0.57$ with frequency Ω for a regular microstructure model with admittance A_y and admittance A_y^r.

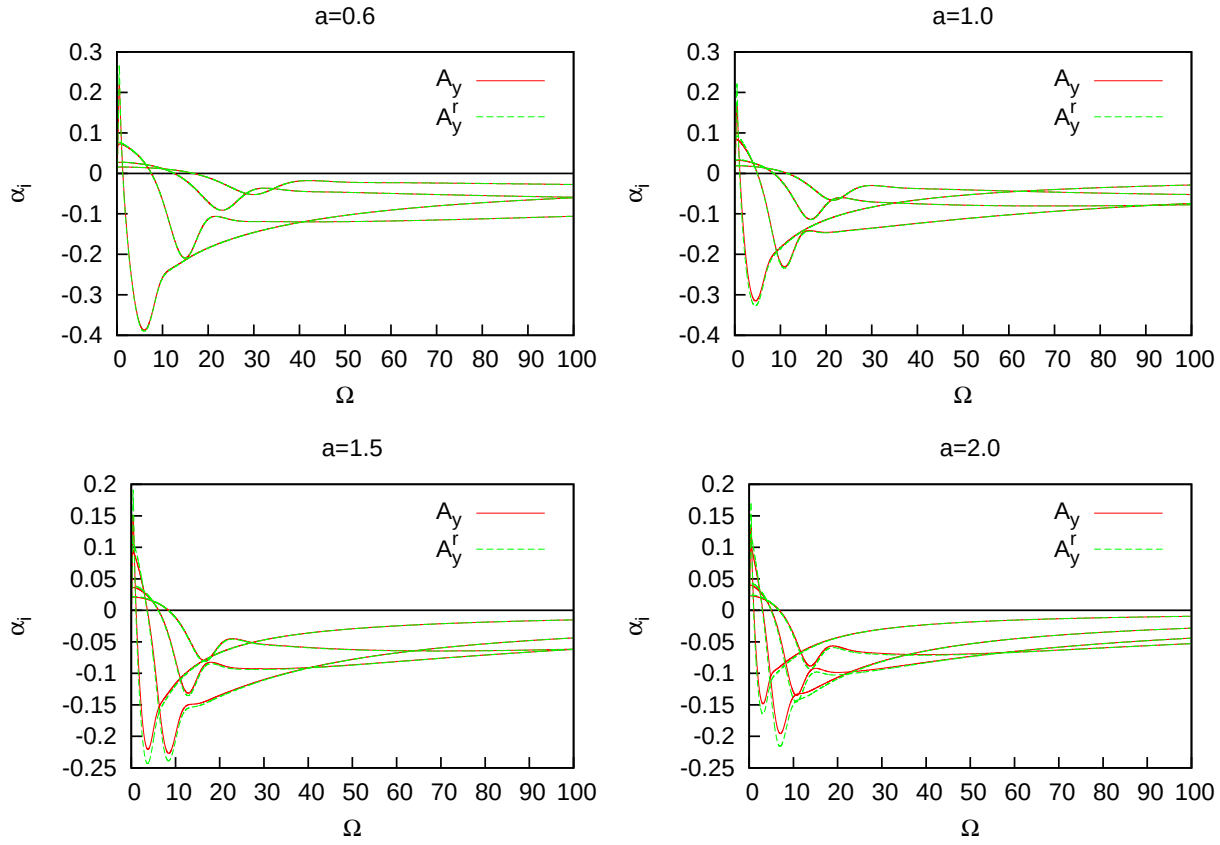

Figure 7: Variation of α_i for $n = 0$ and $a/r_s = 0.57$ with frequency Ω for a regular microstructure model with admittance A_y and admittance A_y^r.

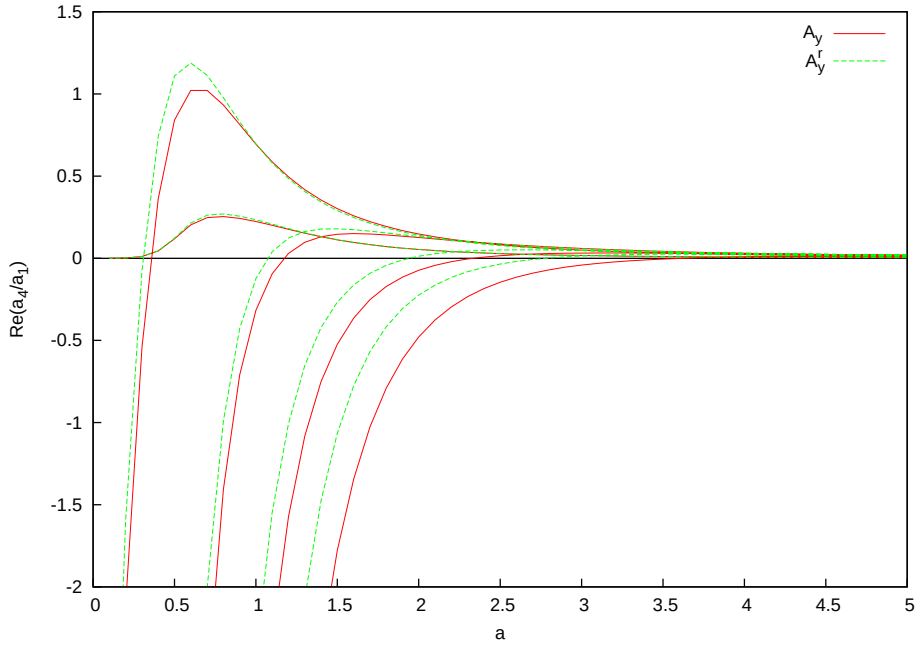

Figure 8: Variation of the nonlinear coefficient $Re(a_4/a_1)$ for $n = 1$ and $a/r_s = 0.57$ with cone radius a for a regular microstructure model with admittance A_y and admittance A_y^r.

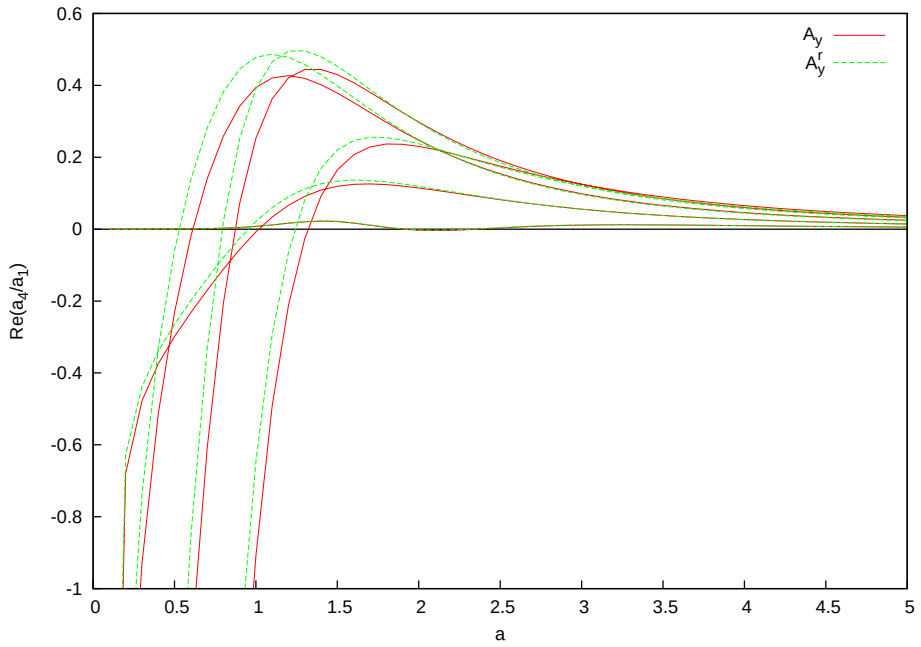

Figure 9: Variation of the nonlinear coefficient $Re(a_4/a_1)$ for $n = 2$ and $a/r_s = 0.57$ with cone radius a for a regular microstructure model with admittance A_y and admittance A_y^r.

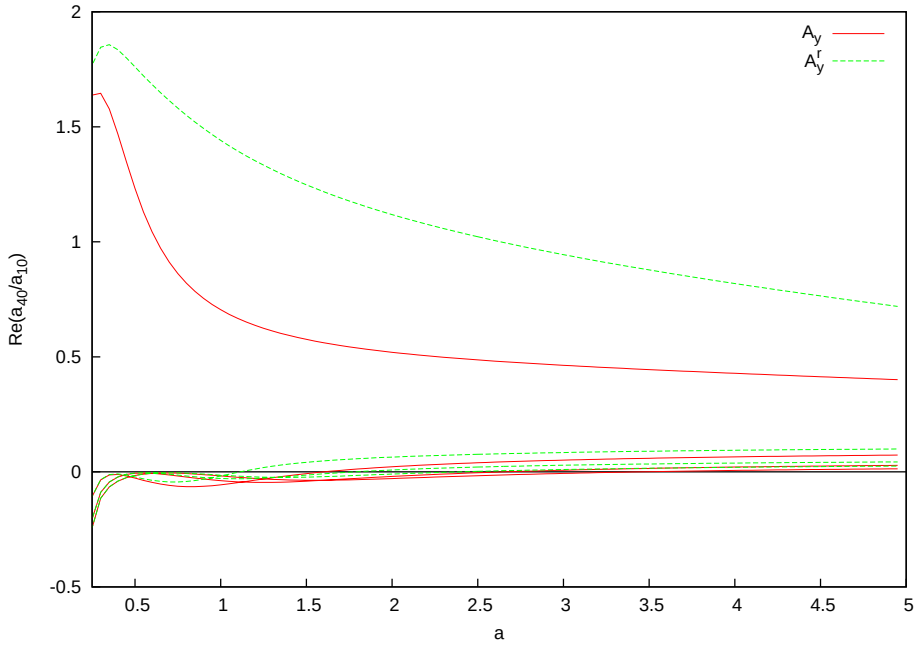

Figure 10: Variation of the nonlinear coefficient $Re(a_4/a_1)$ for $n = 0$ and $a/r_s = 0.57$ with cone radius a for a regular microstructure model with admittance A_y and admittance A_y^r.

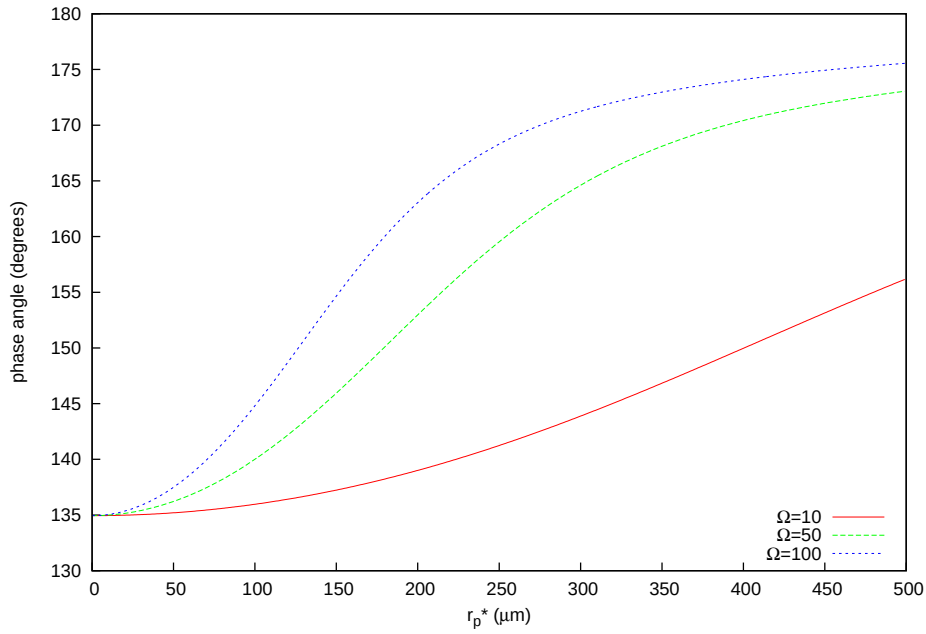

Figure 11: Variation of the phase angle of admittance with pore radius r_p for an infinitely thick porous coating with fixed porosity $\phi_0 = 0.2$

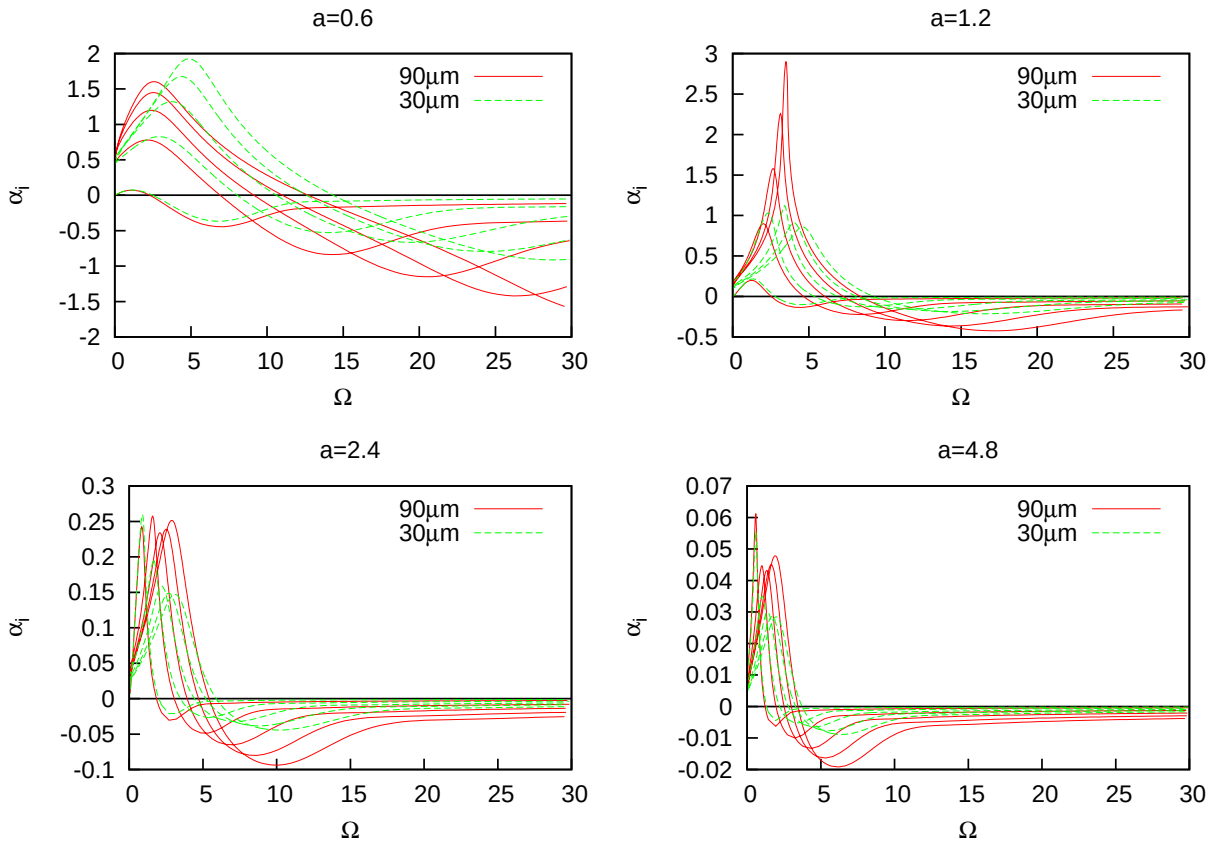

Figure 12: Variation of α_i for $n = 1$ and $a/r_s = 0.57$ with frequency Ω for a regular microstructure model with fixed porosity $\phi_0 = 0.2$ and different pore radii r_p^*.

These theoretical findings are supported by figure 11 which shows the variation of the phase angle with pore radius r_p for three different values of frequency Ω. We can see that for small values of r_p the phase angle tends to $3\pi/4$ for all values of the frequency. As the pore radius increases we see that the phase angle tends towards π particularly for higher values of frequency (which makes $|\zeta|$ larger).

The effect of pore radius on the linear stability of first mode disturbances can be seen in figure 12. We see that increasing the pore radius from 30μm to 90μm leads to a decrease in the cut-off value Ω_c at which the growth rate parameter α_i becomes negative. This effect is more pronounced at smaller values of cone radius a. This means that lower frequencies may become unstable. We can also see that increasing the pore radius also leads to a substantial increase in the maximum growth rates of these linearly unstable disturbances.

We can thus conclude that to avoid deleterious effect of the porous coating on the destabilisation and subsequent nonlinear amplification of first Mack mode disturbances we need to minimize the pore radius so that the phase angle of admittance remains close to $3\pi/4$.

5.2 Effect of porosity and other porous models

In Report 6 of Grant no. FA8655-08-1-3044 the effect of random microstructure porous models on the stability of the first mode was considered. The felt metal significantly destabilises the neutral modes and strongly amplifies the linearly unstable modes with the higher modes giving the largest growth rates [5]. Nonlinear effects in the presence of the felt metal coating stabilise these more dangerous higher modes over a larger range of a while destabilising the more slowly growing lower modes [4]. Since the felt metal coatings have higher porosity compared to typical regular microstructure models, to corroborate these findings, nonlinear stability results for the regular porous model with a higher porosity of $\phi_0 = \frac{\pi}{4}$ was obtained.

In figures 13a and 13b for $n = 0$ and $n = 1$, respectively, we see that higher porosity leads to nonlinearity having a stabilizing effect on mode numbers greater than one. This can be seen by noting the increase in the value of a where $\mathrm{Re}(a_4/a_1)$ becomes positive. However, for large values of a the destabilising effect of nonlinearity is stronger with $\mathrm{Re}(a_4/a_1)$ being slightly larger for higher porosity. In figure 14a for $n = 2$ we see the stabilising effect of higher porosity for mode numbers greater than two and in figure 14b for $n = 3$ we see it for mode numbers greater than three. We may thus conclude that porous coatings with higher porosity allows nonlinear effects to stabilise higher mode number disturbances at a particular location with the mode number of the lowest mode that is stabilised increasing with increasing azimuthal wavenumber.

In Report 6 of Grant no. FA8655-08-1-3044 we also considered the mesh microstructure model which has a high porosity of 0.8. Results from the linear stability analysis was presented. It was shown that the higher porosity of the mesh microstructure only leads to a slightly greater destabilisation of both axisymmetric and non-axisymmetric disturbances when compared to the regular porous model. We now present here the results from the nonlinear stability analysis using the mesh microstructure model and compare it with the regular microstructure model. Figure 15 shows $\mathrm{Re}(a_4/a_1)$ for $n = 1$ for both the models. The effect of the two models on the first mode is similar. For the higher modes nonlinear effects are slightly more destabilising for the regular model compared to the mesh model. This can again be seen by noting that $\mathrm{Re}(a_4/a_1)$ becomes positive at smaller values of a for the regular model compared to the mesh model. Thus the mesh microstructure model provides better performance when compared to both regular and random microstructure coating.

Parametric studies also show that high porosity provides maximum second-mode stabilisation [1]. However numerical studies of Bres *et al.* [7] reveal that porous coatings with too closely spaced pores trigger a new shorter wavelength instability whose growth rate can be larger than that of Mack's second mode. The authors have attempted to optimize the design of porous coatings based on the acoustic scattering properties of the porous layer. They propose a porous coating with fixed low porosity comprising of spanwise grooves. Each porous cavity has a depth H, half-width b and spacing s, all of which vary along the longitudinal length of the cone. Following [13] the regular porous model of (3) can be used to study this

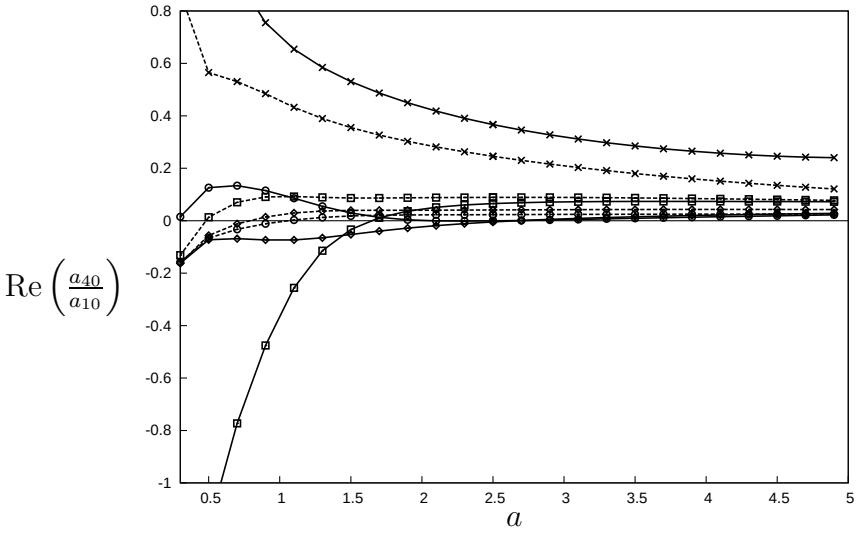

(a)

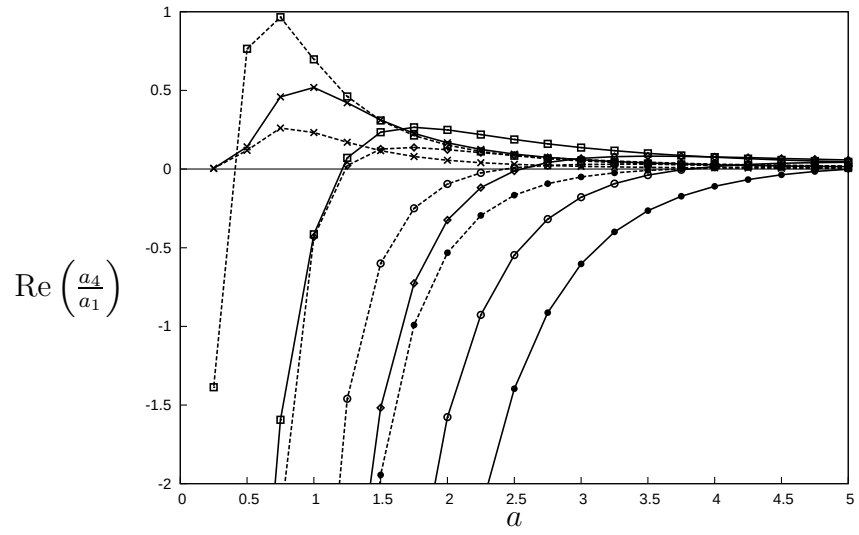

(b)

Figure 13: $\mathrm{Re}(a_4/a_1)$ as a function of local cone radius a for $a/r_s = 0.57$ and (a) $n = 0$; (b) $n = 1$. Results are shown using the regular microstructure model (3): —, $\phi_0 = \pi/4$; − − −, $\phi_0 = 0.2$. Symbols refer to mode number: ×, $m = 1$; □, $m = 2$; ⋄, $m = 3$; ○, $m = 4$; •, $m = 5$.

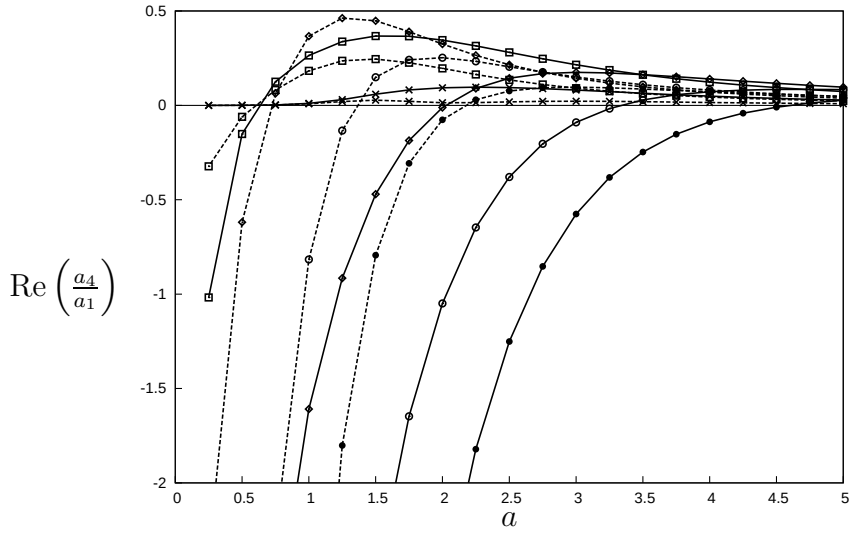

(a)

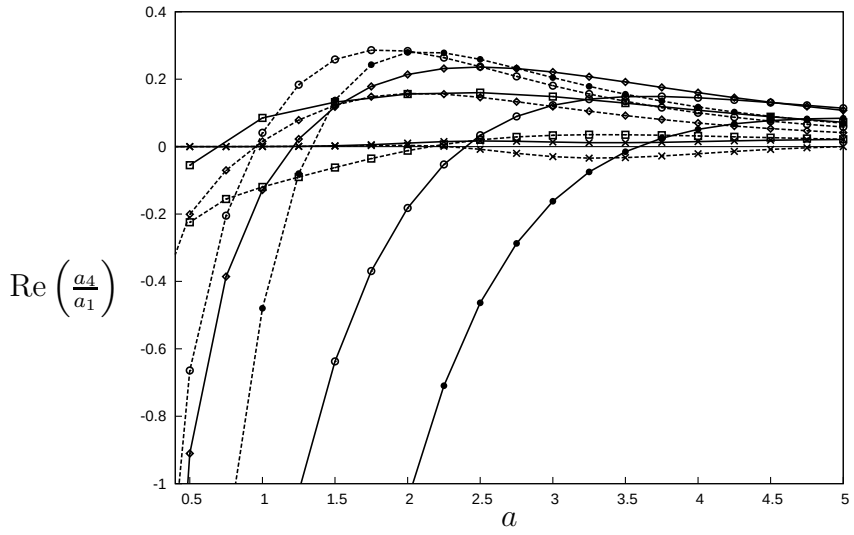

(b)

Figure 14: $\mathrm{Re}(a_4/a_1)$ as a function of local cone radius a for $a/r_s = 0.57$ and (a) $n = 2$; (b) $n = 3$. Results are shown using the regular microstructure model (3): —, $\phi_0 = \pi/4$; − − −, $\phi_0 = 0.2$. Symbols refer to mode number: ×, $m = 1$; □, $m = 2$; ⋄, $m = 3$; ○, $m = 4$; •, $m = 5$.

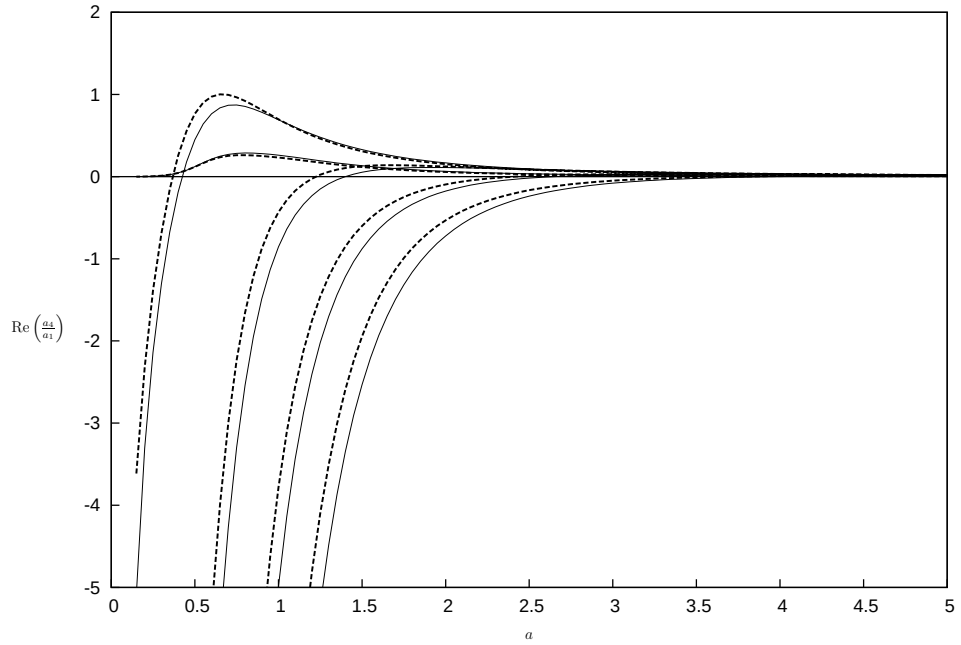

Figure 15: $\mathrm{Re}(a_4/a_1)$ for the first five modes as a function of local cone radius a for $n = 1$ and $a/r_s = 0.57$: —, mesh microstructure model (5); $- - -$, regular microstructure model (3).

model by making the following changes:

$$\zeta = b\sqrt{\frac{\mathrm{i}\omega\rho_w}{\mu_w}R}, \quad F(B,\zeta) = \frac{\tan\zeta}{\zeta[1 - B\zeta\tan\zeta]}. \tag{15}$$

The effect of this new design on the first mode instability is examined. In figure 16 maximum unstable growth rates of the first azimuthal mode $n = 1$ are compared using this porous model and the regular porous model both with porosity $\phi_0 = 0.2$. The regular porous model is assumed to be infinitely thick and the pore radius is fixed at 25μm. From figure 16 we see that at smaller streamwise distance the new design leads to lower amplification of unstable disturbances and with increasing streamwise distance the difference between the growth rates of the two models becomes very small. This novel design corresponds to porous coatings with low porosity and large cavity aspect ratio $(2b/H)$ i.e., thinner coatings with less pores. These type of coatings are easier to manufacture and incorporate into thermal protection systems in hypersonic vehicles [7].

The effect of nonlinearity in the presence of this coating is shown in figure 17. Here we can see $\mathrm{Re}(a_4/a_1)$ against streamwise distance L^* for the spanwise groove model with variable thickness and the regular porous model with infinite thickness. We see that in the presence of the novel porous coating model, nonlinearity has a stabilising effect on all the modes.

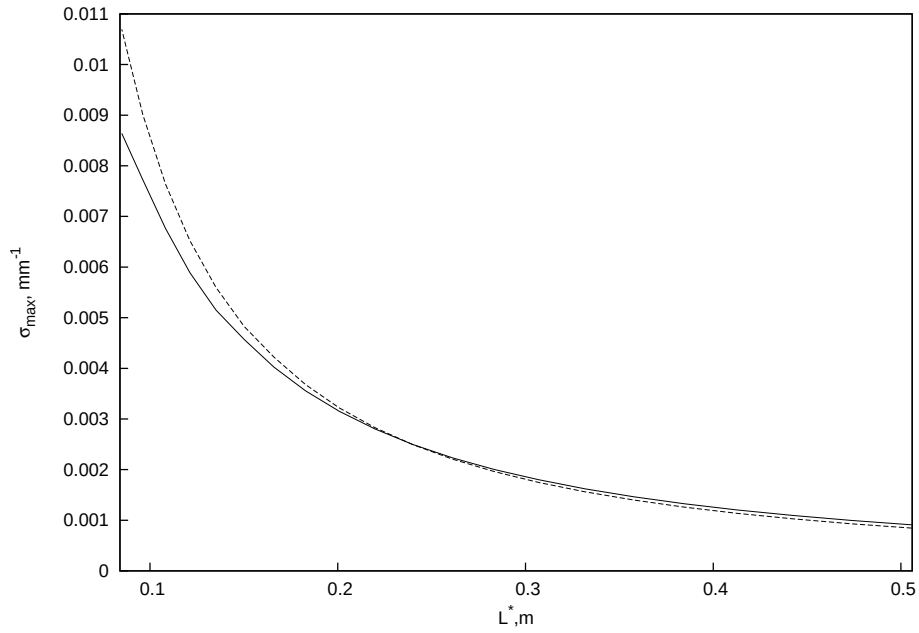

Figure 16: Variation of spatial growth rate parameter $\sigma_{\max} = \max(|-\alpha_i(\Omega)|)$ with longitudinal distance L^*: —, spanwise grooves with variable thickness (5.2); $---$, regular microstructure model (3) with infinite thickness. Results are shown for non-neutral non-axisymmetric mode $n = 1$.

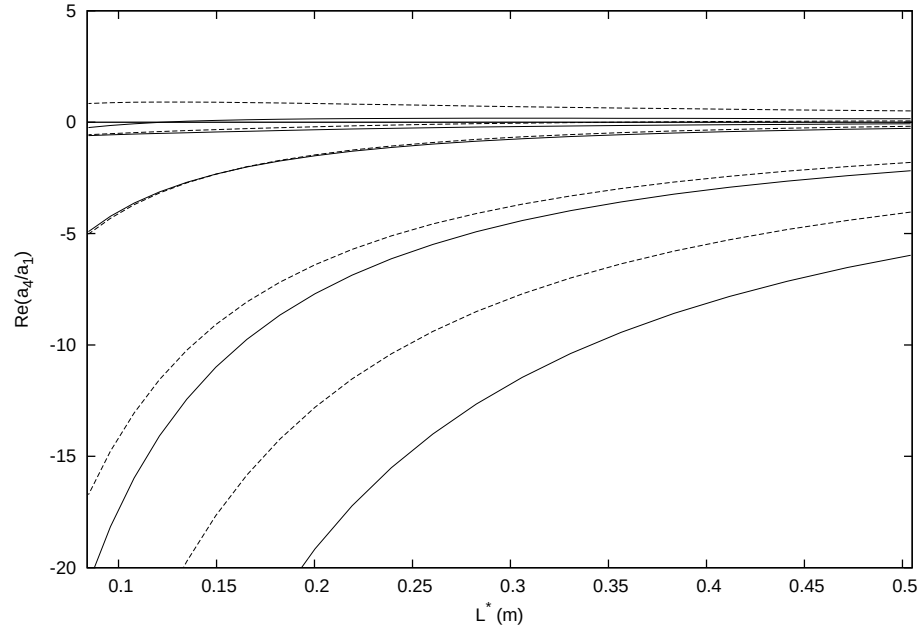

Figure 17: $\mathrm{Re}(a_4/a_1)$ for the first five modes as a function of local cone radius a for $n = 1$ and $a/r_s = 0.57$: —, spanwise grooves with variable thickness (5.2); $---$, regular microstructure model (3) with infinite thickness.

6 Conclusions

In this report we considered the effect of the phase angle of admittance of an infinitely thick regular microstructure porous coating on the linear and weakly nonlinear stability of the first Mack mode. We show that the phase angle significantly affects the nonlinear stability for both axisymmetric and non-axisymmetric disturbances. Our results show that the optimum phase angle of admittance is $3\pi/4$, and this can be achieved by having the pore radius as small as possible.

We then considered the effect of porosity on the stability of the flow. Previous results using random microstructure models and results shown here using regular and mesh microstructure model show that porous coatings with high porosity allow nonlinear effects to stabilise the most linearly unstable modes. These are the higher mode number/frequency modes. However higher porosity can have a detrimental effect on the lower mode number/frequency modes as they are destabilised by nonlinear effects causing a subcritical instability. A novel porous coating with low porosity comprising of spanwise grooves was proposed in [7]. Our results indicate that this type of coating provides optimum performance with regards to both linear and nonlinear stability of first mode disturbances.

References

[1] A. V. Fedorov, N. D. Malmuth, A. Rasheed, and H. G. Hornung. Stabilization of hypersonic boundary layers by porous coatings. *AIAA J.*, 39(4):605–610, 2001.

[2] A. V. Fedorov, A. Shiplyuk, A. A. Maslov, E. Burov, and N. D. Malmuth. Stabilization of a hypersonic boundary layer using an ultrasonically absorptive coating. *J. Fluid Mech.*, 479:99–124, 2003b.

[3] A. V. Fedorov, V. Kozlov, A. Shiplyuk, A. A. Maslov, and N. D. Malmuth. Stability of hypersonic boundary layer on porous wall with regular microstructure. *AIAA Journal*, 44(8):1866–1871, 2006.

[4] V. Michael and S. O. Stephen. Nonlinear stability of hypersonic flow over a cone with passive porous walls. *J. Fluid Mech.*, 713:528–563, 2012.

[5] S. O. Stephen and V. Michael. Effects of porous walls on hypersonic boundary layers over a sharp cone. *AIAA J.* To appear.

[6] X. Wang and X. Zhong. Phase angle of porous coating admittance and its effect on boundary-layer stabilization. *AIAA Paper 2011-3080*, 2011b.

[7] G. A. Bres, M. Inkman, T. Colonius, and A. V. Fedorov. Alternate designs of ultrasonic absorptive coatings for hypersonic boundary layer control. *AIAA Paper 2009-4217*, 2009.

[8] S. O. Seddougui and A. P. Bassom. Instability of hypersonic flow over a cone. *J. Fluid Mech.*, 345:383–411, 1997.

[9] M. Rasmussen. *Hypersonic flow*. Wiley Interscience, 1994.

[10] W. D. Hayes and R. Probstein. *Hypersonic Inviscid Flows*. Dover, 2004.

[11] A. A. Maslov. Experimental and theoretical studies of hypersonic laminar flow control using ultrasonically absorptive coatings (UAC). Technical Report ISTC 2172-2001, International Science and Technology Centre, 2003.

[12] S. V. Lukashevich, A. A. Maslov, A. N. Shiplyuk, A. V. Fedorov, and V. G. Soudakov. Stabilization of high-speed boundary layer using porous coatings of various thicknesses. *AIAA Paper 2010-4720*, 2010.

[13] V. F. Kozlov, A. V. Fedorov, and N. D. Malmuth. Acoustic properties of rarefied gases inside pores of simple geometries. *J. Acoust. Soc. Am.*, 117(6):3402–3412, 2005.

[14] S. J. Cowley and P. Hall. On the instability of hypersonic flow past a wedge. *J. Fluid Mech.*, 214:17–42, 1990.

[15] P. W. Duck and P. Hall. Non-axisymmetric viscous lower-branch modes in axisymmetric supersonic flows. *J. Fluid Mech.*, 213:191–201, 1990.

[16] S. O. Seddougui. Stability of hypersonic flow over a cone. In M. Y. Hussaini, T. B. Gatski, and T. L. Jackson, editors, *Transition, Turbulence and Combustion*, pages 50–59. Kluwer, 1994a.

[17] P. W. Duck and P. Hall. On the interaction of Tollmien-Schlichting waves in axisymmetric supersonic flows. *Q. J. Mech. App. Maths*, 42:115–130, 1989.

[18] F. T. Smith. Nonlinear stability of boundary layers for disturbances of various sizes. *Proc. R. Soc. A*, 368:573–589, 1979a. See also A 371 (1980) 439-440.

[19] P. Hall and F. T. Smith. A suggested mechanism for nonlinear wall roughness effects on high Reynolds number flow stability. *Stud. Appl. Math.*, 66:241–265, 1982.

7 List of Symbols, Abbreviations, and Acronyms

a	=	cone radius
$\widetilde{a}$	=	half-pore width
b	=	pore groove width
A	=	displacement function
A_y	=	admittance
$\overline{A_Y}$	=	scaled admittance
C_D	=	$C_D^* \gamma p_-$, dynamic compressibility
d^*	=	fibre diameter
h_0	=	porous-layer thickness
H	=	porous-layer thickness
L^*	=	length scale
Kn	=	Knudsen number
M	=	Mach number
n	=	azimuthal wavenumber
Pr	=	Prandtl number
P	=	pressure disturbance
R	=	$U_- \delta^* / \nu_-$, Reynolds number
Re	=	Reynolds number
r_p	=	pore radius
r_s	=	shock location
T	=	temperature
u, v	=	velocity disturbance
x, $\overline{r}$, ϕ	=	orthogonal coordinates
Z_0	=	characteristic impedance
α	=	streamwise wavenumber
γ	=	specific heat ratio
δ^*	=	boundary-layer displacement thickness
θ_c	=	cone angle
θ_s	=	shock angle
Λ	=	propagation constant
Ω	=	frequency
μ	=	viscosity
ν	=	kinematic viscosity
ρ	=	density
ρ_D	=	ρ_D^* / ρ_W^*, dynamic density
ϕ_0	=	porosity
σ^*	=	flow resistivity
ω	=	angular frequency
λ	=	skin friction

Subscripts

$-$	=	just behind the shock
s	=	shock
w	=	wall
i	=	imaginary part

Superscripts

$*$	=	dimensional term
r	=	real quantity